Weierstraß-Institut
für Angewandte Analysis und Stochastik
Leibniz-Institut im Forschungsverbund Berlin e. V.

Preprint   ISSN 2198-5855

On spurious oscillations due to irrotational forces in the Navier–Stokes momentum balance

Alexander Linke[1], Christian Merdon[1]

submitted: June 22, 2015

[1]   Weierstrass Institute
     Mohrenstr. 39
     10117 Berlin
     Germany
     email: Alexander.Linke@wias-berlin.de
            Christian.Merdon@wias-berlin.de

No. 2132

Berlin 2015

ABSTRACT. This contribution studies the influence of the pressure on the velocity error in finite element discretisations of the Navier-Stokes equations. Three simple benchmark problems that are all close to real-world applications convey that the pressure can be comparably large and is not to be underestimated. For widely used finite element methods like the Taylor-Hood finite element method, such relatively large pressures can lead to spurious oscillations and arbitrarily large errors in the velocity, even if the exact velocity is in the ansatz space. Only mixed finite element methods, whose velocity error is pressure-independent, like the Scott-Vogelius finite element method can avoid this influence.

1. INTRODUCTION

Often, spurious velocity oscillations in discretisations of the incompressible Navier–Stokes equations are attributed to dominant convection at high Reynolds numbers, like in the case of *scalar* singularly perturbed advection-diffusion equations. However, spurious velocity oscillations can also be excited by a different mechanism, which can only appear in *vector equations*: the lack of L^2-orthogonality of (only) discretely divergence-free vector fields and large gradient fields in the Navier–Stokes momentum balance [Lin14]. This lack of L^2-orthogonality makes the velocity error of mixed finite elements like the Taylor–Hood element for the incompressible (Navier–)Stokes equations *pressure-dependent*, i.e. $C_2 = 1$ in

$$(1) \qquad \|\nabla(\mathbf{u} - \mathbf{u}_h)\|_0 \leqslant C_1 \inf_{\mathbf{w} \in V(\mathcal{T})} \|\nabla(\mathbf{u} - \mathbf{w}_h)\|_0 + \frac{C_2}{\nu} \inf_{q_h \in Q(\mathcal{T})} \|p - q_h\|_0,$$

which can be found in textbooks like [GR86, BF91]. Although mixed finite elements like the Scott–Vogelius element exist, whose velocity error is *pressure-independent* ($C_2 = 0$), traditionally the pressure-dependence of the velocity error of many flow discretisations seems to be regarded of secondary importance. More or less, common belief in the numerical analysis community is that convergence of asymptotically optimal order would be sufficient for potential success in real-world flow problems.

However, we want to emphasize in this contribution that there is an assumption hidden in this belief: the pressure has to be comparably small and may not be too complicated, since otherwise the pressure-dependent part of the velocity error would be dominant and the constant C_2/ν in error estimate (1) could be arbitrarily large, depending on the flow problem. In order to practically demonstrate that the assumption of a small and simple pressure is generally wrong in real-world applications, we present three simple benchmarks, where the pressure is *large w.r.t. the velocity* and the velocity will be an (at most) linear vector field. In the first benchmark, a buoyancy force exactly balances the pressure gradient (momentum balance: $\nabla p = \mathbf{f}$), yielding a hydrostatic situation. In the second benchmark, a strong y-dependent Coriolis force balances the pressure gradient (momentum balance: $2\boldsymbol{\omega} \times \mathbf{u} + \nabla p = \mathbf{0}$), as it appears in large-scale flows in the so-called β-plane approximation in meteorology [Ped92]. In the third benchmark, the nonlinear convection term $(\mathbf{u} \cdot \nabla)\mathbf{u}$ is balanced by the pressure gradient in a rigid-body-rotation (momentum balance: $(\mathbf{u} \cdot \nabla)\mathbf{u} + \nabla p = \mathbf{0}$). These examples demonstrate that the error contribution $\frac{C_2}{\nu} \inf_{q_h \in Q(\mathcal{T})} \|p - q_h\|_0$ appears in all kinds of incompressible flows and can have a major influence on the velocity error. In fact, in all three

examples, this error contribution is the *only error source*, since the continuous velocity solution lies in the discrete velocity space.

Since the pressure is in all three examples comparably large, low-order mixed finite element methods on unstructured grids like the Taylor–Hood finite element method will heavily suffer from spurious velocity oscillations. Instead, the Scott–Vogelius finite element method or novel modified finite element methods such as [Lin14, LMT14, BLMS15], whose velocity errors are *pressure-independent*, i.e. $C_2 = 0$ in (1), will be able to deliver the exact velocity solution.

The third example, where the nonlinear convection term balances the pressure gradient, is especially important. In this example, spurious velocity oscillations are excited, when the Reynolds number becomes large, though they are not excited by dominant advection. We remind the reader that even unstable Galerkin discretisations for singularly perturbed advection-diffusion equations deliver the exact solution, whenever it lies in the discrete trial space. Moreover, spurious oscillations due to dominant convection are only excited in the presence of (interior or boundary) layers, which our example does not have. Therefore, the third benchmark delivers a simple and highly didactic example demonstrating that the nonlinear convection term excites two different kinds of spurious velocity oscillations at high Reynolds numbers. This argument was made recently in [Lin09], but it does not seem to be widely acknowledged by the CFD community, though its importance for the discretisation of the nonlinear convection term is potentially high.

2. The Navier-Stokes Model Problem and its Discretisation

This section recalls the Navier-Stokes equations with Coriolis force and its discretisation with finite element methods.

2.1. **The Navier-Stokes Equations.** The Navier-Stokes equations with angular velocity ω, right-hand side $\mathbf{f}$ and Dirichlet data $\mathbf{u}_D$ for some $d \in \{2,3\}$ dimensional bounded Lipschitz domain Ω with polygonal boundary $\partial\Omega$ read

$$(2) \quad -\nu\Delta\mathbf{u} + (\mathbf{u}\cdot\nabla)\mathbf{u} + \nabla p + 2\omega\times\mathbf{u} = f, \qquad \nabla\cdot\mathbf{u} = 0, \qquad \mathbf{u} = \mathbf{u}_D \quad \text{along } \partial\Omega.$$

The weak formulation employs the multilinear forms

$$a(\mathbf{u}, \vec{v}) := \int_{\mathcal{T}} \nu\nabla\mathbf{u} : \nabla\mathbf{v} \ dx, \qquad\qquad b(\mathbf{u}, q) := -\int_{\Omega} q\nabla\cdot\mathbf{u} \ dx,$$

$$c(\mathbf{u}, q) := \int_{\Omega} (2\omega\times\mathbf{u})\cdot\mathbf{v} \ dx, \qquad\qquad d(\mathbf{a}, \mathbf{u}, \mathbf{v}) := \int_{\Omega} ((\mathbf{a}\cdot\nabla)\mathbf{u})\cdot\mathbf{v} \ dx,$$

$$F(\mathbf{v}) := \int_{\Omega} \mathbf{f}\cdot\mathbf{v} \ dx$$

and characterises weak solutions $(\mathbf{u}, p) \in H^1(\Omega; \mathbb{R}^d) \times L_0^2(\Omega)$ of (2) by $\mathbf{u} = \mathbf{u}_D$ along $\partial\Omega$ and

$$(3) \qquad a(\mathbf{u}, \mathbf{v}) + d(\mathbf{u}, \mathbf{u}, \mathbf{v}) + b(\mathbf{v}, p) + c(\mathbf{u}, \mathbf{v}) = F(\mathbf{v}) \quad \text{for all } \mathbf{v}_h \in V := H_0^1(\Omega; \mathbb{R}^d),$$
$$b(\mathbf{u}, q) = 0 \quad \text{for all } q_h \in Q := L_0^2(\Omega).$$

2.2. **Taylor-Hood and Scott-Vogelius Finite Element Method.** The finite element discretisations below employ a regular triangulation $\mathcal{T}$ of the domain Ω into triangles ($d = 2$) or tetrahedra ($d = 3$) and replace V and Q in (3) by discrete subspaces $V(\mathcal{T})$ and $Q(\mathcal{T})$ that satisfy the inf-sup stability condition

$$(4) \qquad 0 < \beta := \inf_{q_h \in Q(\mathcal{T})\backslash\{0\}} \sup_{\mathbf{v}_h \in V(\mathcal{T})\backslash\{0\}} \frac{b(\mathbf{v}_h, q_h)}{\|\nabla\mathbf{v}_h\|_0 \|q_h\|_0}.$$

To ensure antisymmetry of the nonlinear term when tested with discrete test functions, the trilinear-form d is replaced by

$$d_h(\mathbf{a}, \mathbf{u}, \mathbf{v}) := \left(\int_{\Omega} ((\mathbf{a}\cdot\nabla_h)\mathbf{u})\cdot\mathbf{v} \ dx - \int_{\Omega} ((\mathbf{a}\cdot\nabla_h)\mathbf{v})\cdot\mathbf{u} \ dx \right)/2.$$
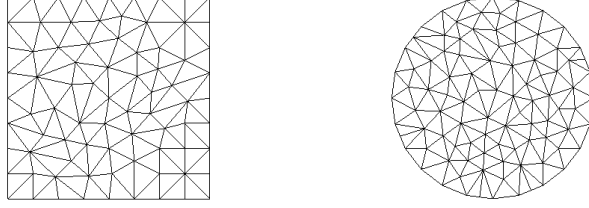
FIGURE 1. Example meshes for the unit square (left) and the unit disk (right).

Then, the finite element method seeks $\mathbf{u}_h \in V(\mathcal{T})$ and $p_h \in Q(\mathcal{T})$ such that $\mathbf{u} = \mathbf{u}_D$ along $\partial\Omega$ and

(5)
$$a_h(\mathbf{u}_h, \mathbf{v}_h) + d_h(\mathbf{u}_h, \mathbf{u}_h, \mathbf{v}_h) + b_h(\mathbf{v}_h, p_h) + c_h(\mathbf{u}_h, \mathbf{v}_h) = F(\mathbf{v}_h) \quad \text{for all } \mathbf{v}_h \in V(\mathcal{T}) \cap H_0^1(\Omega),$$
$$b_h(\mathbf{u}_h, q_h) = 0 \quad \text{for all } q_h \in Q(\mathcal{T}).$$

The test function spaces for the Taylor-Hood finite element method read

$$V(\mathcal{T}) := \mathrm{TH}(\mathcal{T}; \mathbb{R}^d) := P_2(\mathcal{T}; \mathbb{R}^d) \cap H^1(\Omega; \mathbb{R}^d),$$
$$Q(\mathcal{T}) := \left\{ q_h \in P_1(\mathcal{T}) \cap H^1(\Omega) : \int_\Omega p_h \, dx = 0 \right\}.$$

The test function spaces for the Scott-Vogelius finite element method read

$$V(\mathcal{T}) := \mathrm{SV}(\mathcal{T}; \mathbb{R}^d) := P_d(\mathcal{T}_B; \mathbb{R}^d) \cap H^1(\Omega; \mathbb{R}^d),$$
$$Q(\mathcal{T}) := \left\{ q_h \in P_{d-1}(\mathcal{T}_B) : \int_\Omega p_h \, dx = 0 \right\}.$$

Here, $\mathcal{T}_B$ denotes a barycentric refinement of the triangulation that ensures inf-sup stability of $V(\mathcal{T})$ and $Q(\mathcal{T})$ in case of the Scott-Vogelius finite element method [Qin94, Zha05]. Unfortunately, this makes the Scott-Vogelius finite element method expensive. On the other hand the property $\nabla \cdot V(\mathcal{T}) \subseteq Q(\mathcal{T})$ implies that the Scott-Vogelius solution $\mathbf{u}_h \in \mathrm{TH}(\mathcal{T}; \mathbb{R}^d)$ is divergence-free, while the discrete solution $\mathbf{u}_h \in \mathrm{TH}(\mathcal{T}; \mathbb{R}^d)$ of the Taylor-Hood finite element method is in general not divergence-free.

3. Real-World Benchmark Examples

The following three examples study (simplified) real-world situations where realistic pressures lead to significant velocity oscillations in the discrete solution of classical mixed finite element methods, although the exact solution is in the velocity ansatz space. Figure 1 displays typical meshes used in the examples.

3.1. **Hydrostatic Situation.** The first example studies a buoyancy force $\mathbf{f} = \nabla p$ that exactly balances the gradient of the pressure $p(x, y) := y^2 - 1/3$ for $\Omega := (0,1)^2$ and $\nu = 1$, yielding a hydrostatic situation with $\mathbf{u} \equiv 0$. Such a flow arises in the Oberbeck–Boussinesq approximation of thermally-driven flows [Ped92], whenever the Rayleigh-number is comparably small. Here, the buoyancy forcing $\mathbf{f}(x, y) = (0, 2y)^T$ appears when the temperature distribution in the flow obeys $T(x, y) = y$.

Tables 1 and 2 show that the Scott-Vogelius finite element method (with $C_2 = 0$!) computes the exact velocity solution, while the Taylor-Hood finite element method shows errors in the velocity on unstructured meshes although $\mathbf{u} \in V(\mathcal{T})$. This is due to the pressure contribution in the a priori error estimates. Moreover, the errors can be made arbitrarily large by reducing the viscosity parameter ν as shown in Figure 2.

ndof	$\|\mathbf{u} - \mathbf{u}_h\|_0$	$\|\nabla(\mathbf{u} - \mathbf{u}_h)\|_0$	$\|p - p_h\|_0$	$\|\nabla \cdot \mathbf{u}_h\|_0$
186	2.1564e-15	1.9151e-14	9.2128e-03	7.1148e-15
664	1.1571e-15	1.1767e-14	2.6854e-03	4.7025e-15
2712	1.0178e-15	9.5467e-15	6.1131e-04	4.0432e-15
10397	9.9598e-16	8.9622e-15	1.5570e-04	3.8523e-15
order	-	-	2.0163	-

TABLE 1. Results for Scott-Vogelius FEM in Section 3.1.

ndof	$\|\mathbf{u} - \mathbf{u}_h\|_0$	$\|\nabla(\mathbf{u} - \mathbf{u}_h)\|_0$	$\|p - p_h\|_0$	$\|\nabla \cdot \mathbf{u}_h\|_0$
178	9.6944e-05	1.9391e-03	5.6969e-03	1.6500e-03
650	1.8501e-05	6.7852e-04	1.3821e-03	6.4252e-04
2361	2.4460e-06	1.7847e-04	3.5466e-04	1.6629e-04
9280	3.3253e-07	4.7348e-05	9.1917e-05	4.4571e-05
order	2.9704	1.9829	2.0085	1.9761

TABLE 2. Results for Taylor-Hood FEM in Section 3.1 for $\nu = 1$.
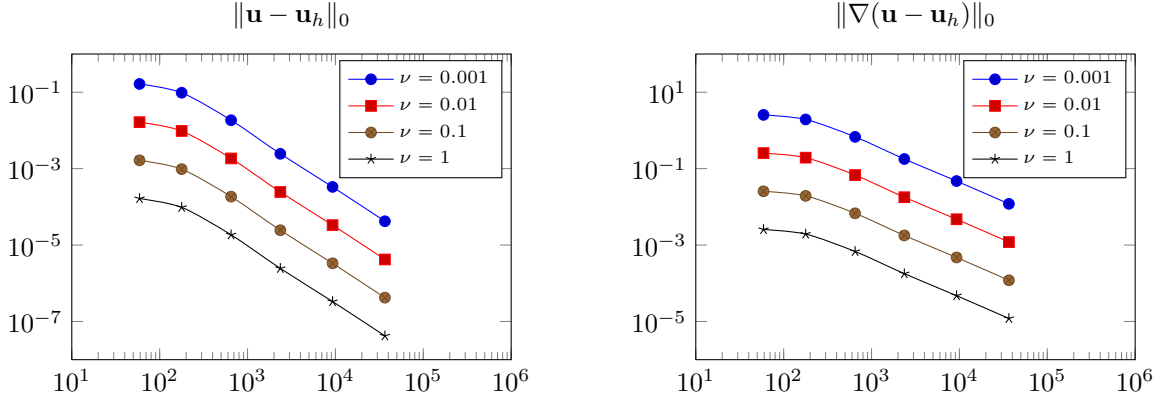
$\|\mathbf{u} - \mathbf{u}_h\|_0$ $\|\nabla(\mathbf{u} - \mathbf{u}_h)\|_0$

FIGURE 2. Convergence history of the L^2 velocity error (left) and the velocity gradient error (right) of the Taylor-Hood finite element method versus the number of degrees of freedom in Section 3.1 for different values of ν.
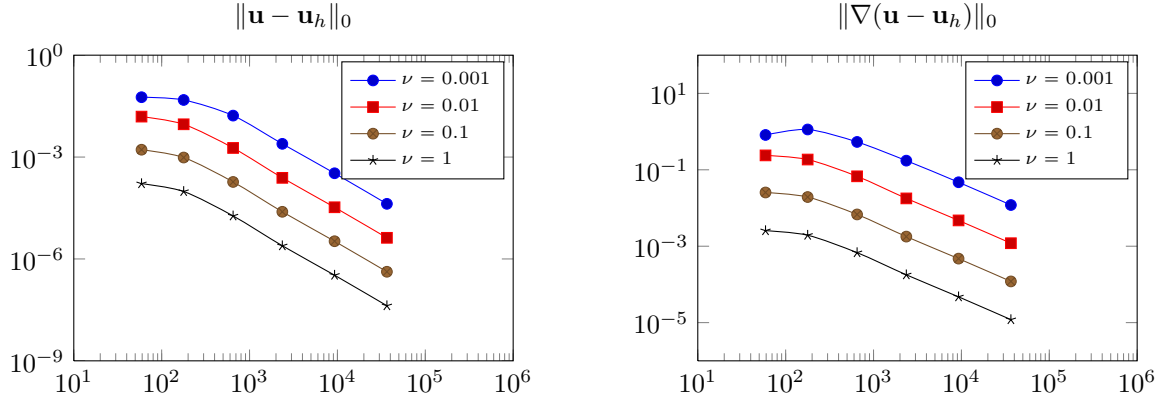
ndof	$\|\mathbf{u} - \mathbf{u}_h\|_0$	$\|\nabla(\mathbf{u} - \mathbf{u}_h)\|_0$	$\|p - p_h\|_0$	$\|\nabla \cdot \mathbf{u}_h\|_0$
186	2.2287e-15	2.4318e-14	9.2128e-03	9.5907e-15
664	1.3990e-15	2.3625e-14	2.6854e-03	9.0401e-15
2712	8.9699e-16	2.6682e-14	6.1131e-04	1.0068e-14
10397	2.2350e-15	4.8028e-14	1.5570e-04	1.9672e-14
order	-	-	1.9572	-

TABLE 3. Results for Scott-Vogelius FEM in Section 3.2.

3.2. **Position-Dependent Coriolis Force.** This example considers the Stokes equations on the unit square $\Omega := (0,1)^2$ with Coriolis force and vanishing right-hand side $\mathbf{f} \equiv 0$ for the constant inflow $\mathbf{u} := (1,0)$ (a simple "west wind"). The y-dependency of the angular velocity $\boldsymbol{\omega}(x,y) := (0,0,\beta_0 y)$ requires the quadratic pressure $p := \beta_0(y^2 - 1/3)$ to obtain $\nabla p + 2\omega \times \mathbf{u} = 0$. Tables 3 and 4 show the numerical results for $\beta_0 = \nu = 1$. Again, the Scott-Vogelius finite element is able to produce the exact velocity solution, while the velocity of the Taylor-Hood finite element method is polluted by the pressure error. Figure 3 shows the increase of the velocity error for $\nu \to 0$.

3.3. **Nonlinear Convection in Rigid Body Rotation.** This example considers the Navier-Stokes equations on the unit disk $\Omega := \{(x,y) \in \mathbb{R}^2 : x^2 + y^2 \leqslant 1\}$ without Coriolis force and vanishing right-hand side $\mathbf{f} \equiv 0$ for the circular flow $\mathbf{u}(x,y) := (-y,x)$. These conditions lead to the quadratic

ndof	$\|\mathbf{u} - \mathbf{u}_h\|_0$	$\|\nabla(\mathbf{u} - \mathbf{u}_h)\|_0$	$\|p - p_h\|_0$	$\|\nabla \cdot \mathbf{u}_h\|_0$
178	9.6948e-05	1.9391e-03	5.6970e-03	1.6501e-03
650	1.8501e-05	6.7852e-04	1.3821e-03	6.4252e-04
2361	2.4460e-06	1.7847e-04	3.5466e-04	1.6629e-04
9280	3.3253e-07	4.7348e-05	9.1917e-05	4.4571e-05
order	3.0493	2.0244	2.0442	2.0246

TABLE 4. Results for Taylor-Hood FEM in Section 3.2 for $\nu = 1$.

FIGURE 3. Convergence history of the L^2 velocity error (left) and the velocity gradient error (right) of the Taylor-Hood finite element method versus the number of degrees of freedom in Section 3.2 for different values of ν.

ndof	$\|\mathbf{u} - \mathbf{u}_h\|_0$	$\|\nabla(\mathbf{u} - \mathbf{u}_h)\|_0$	$\|p - p_h\|_0$	$\|\nabla \cdot \mathbf{u}_h\|_0$
893	2.5245e-14	4.4558e-13	2.1032e-02	1.3410e-13
3399	1.4493e-13	4.4160e-12	5.4896e-03	1.0879e-12
12638	1.5208e-14	9.9279e-13	1.3949e-03	2.5477e-13
52469	9.2076e-15	8.1960e-13	3.4659e-04	2.2274e-13
order	-	-	2.0291	-

TABLE 5. Results for Scott-Vogelius FEM in Section 3.3.

ndof	$\|\mathbf{u} - \mathbf{u}_h\|_0$	$\|\nabla(\mathbf{u} - \mathbf{u}_h)\|_0$	$\|p - p_h\|_0$	$\|\nabla \cdot \mathbf{u}_h\|_0$
791	7.8827e-05	1.7420e-03	6.3646e-03	1.6602e-03
2835	1.1488e-05	4.8856e-04	1.6382e-03	4.7153e-04
11451	1.3543e-06	1.1763e-04	4.0255e-04	1.1368e-04
45256	1.7825e-07	3.0921e-05	1.0175e-04	2.9842e-05
order	2.9961	2.0015	2.0096	2.0006

TABLE 6. Results for Taylor-Hood FEM in Section 3.3 for $\nu = 1$.

pressure $p := (x^2 + y^2)/2 - 1/4$ that balances the nonlinear term, i.e. $\nabla p + (\mathbf{u} \cdot \nabla)\mathbf{u} = 0$. Tables 5 and 6 show the numerical results for $\nu = 1$. Also in this example, the Scott-Vogelius finite element computes the exact velocity solution, while the Taylor-Hood finite element method does not. Figure 4 shows the increase of the velocity error for $\nu \to 0$.
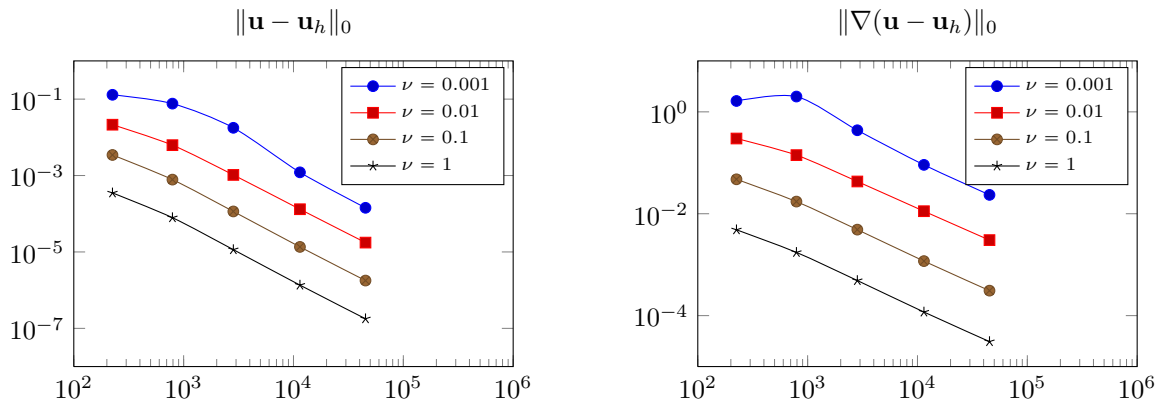
FIGURE 4. Convergence history of the L^2 velocity error (left) and the velocity gradient error (right) of the Taylor-Hood finite element method versus the number of degrees of freedom in Section 3.3 for different values of ν.

REFERENCES

[BF91]   Franco Brezzi and Michel Fortin, *Mixed and hybrid finite element methods*, Springer-Verlag New York, Inc., New York, NY, USA, 1991.

[BLMS15] C. Brennecke, A. Linke, C. Merdon, and J. Schöberl, *Optimal and pressure-independent L^2 velocity error estimates for a modified Crouzeix-Raviart Stokes element with BDM reconstructions*, J. Comput. Math. **33** (2015), no. 2, 191–208.

[GR86]   V. Girault and P.-A. Raviart, *Finite element methods for Navier-Stokes equations*, Springer Series in Computational Mathematics, vol. 5, Springer-Verlag, Berlin, 1986.

[Lin09]   A. Linke, *Collision in a cross-shaped domain – a steady 2d navierstokes example demonstrating the importance of mass conservation in CFD*, Computer Methods in Applied Mechanics and Engineering **198** (2009), no. 41–44, 3278–3286.

[Lin14]   Alexander Linke, *On the role of the Helmholtz decomposition in mixed methods for incompressible flows and a new variational crime*, Comput. Methods Appl. Mech. Engrg. **268** (2014), 782–800. MR 3133522

[LMT14]   A. Linke, G. Matthies, and L. Tobiska, *Robust arbitrary order mixed finite element methods for the incompressible stokes equations*, WIAS Preprint (2014), no. 2027.

[Ped92]   J. Pedlosky, *Geophysical fluid dynamics*, Springer study edition, Springer New York, 1992.

[Qin94]   J. Qin, *On the convergence of some low order mixed finite elements for incompressible fluids*, Ph.D. thesis, Pennsylvania State University, 1994.

[Zha05]   S. Zhang, *A new family of stable mixed finite elements for the 3d Stokes equations*, Math. Comp. **74** (2005), no. 250, 543–554.